A Multiple Direction Radiation Sensor, DIRAM

J. C. H. VAN DER HAGE, H. VAN DOP, A. LOS, W. BOOT, AND D. VAN AS

Institute for Marine and Atmospheric Sciences, Utrecht University, Utrecht, Netherlands

(Manuscript received 18 April 2000, in final form 27 January 2001)

ABSTRACT

The Directional Radiance Distribution Measurement (DIRAM) device was designed and built to determine the angular distribution of shortwave radiance as a function of height in cloudy and clear-sky conditions at various surface albedos. The construction contains 42 sensors, consisting of a collimation system and a detector, which are mounted in two domes (21 in each). The collimators are made of solid PERSPEX cylinders, 8 mm in diameter and ~24 mm long, which are fully transparent in the visible range. Three diaphragms are carved in each cylinder to reduce the field of view to ~7° and to reduce the stray light. The detector is a commerially available silicon photodiode for the visible spectral range. The domes can be placed at ground level, or on top and below a research aircraft. The collimators collect broadband visible radiation in 42 regularly distributed viewing angles. The aperture of each sensor is about 7°. The 42 signals are continuously stored by a datalogger with variable frequency up to 10 Hz. The angular dependence of solar radiation scattered from clouds (or the earth's surface) can be determined. The purpose is to collect data on the scattering of solar radiation by clouds (and surface) in order to gain more insight in the shortwave atmospheric radiation budget. Optical properties such as angular discrimination of the collimators and sensitivity of the device were investigated and summarized. During a test flight the operational aspects were investigated. It appeared that the device was able to collect data without interruption in severe conditions (vibrations, strong temperature, and humidity changes).

1. Introduction

a. Clouds and radiation

Atmospheric radiation is strongly influenced by clouds. Since the former determines climate on earth, clouds are major actors in all climate studies, the more so since the radiation budget is very sensitive to small variations in cloud cover and characteristics. Most modeling and observational efforts related to climate concern the net upwelling radiation, which is a complex convolution of radiative scattering and absorption processes in clear sky, clouds, and at the earth's surface. The description of these complex processes contains numerous uncertainties of microphysical (single photon scattering by liquid water, aerosol particles, and ice crystals) and macrophysical (vertical and horizontal inhomogeneity in cloud distribution and composition) nature, which still inhibit an accurate assessment of the climate impact.

In atmospheric modeling of radiation transfer, clouds are often represented as extended homogeneous layers of constant thickness. Homogeneity is assumed in for example, droplet size, liquid water content, and droplet number concentration. In reality these quantities may strongly vary on all scales, even in stratiform cloud types. This variance in cloud properties has a distinct influence on the radiation transfer process (Los and Duynkerke 2001). One of the consequences is that the horizontal divergence of radiative fluxes cannot always be neglected. Also, in regions with scattered clouds, a full 3D analysis of radiation transfer is required. The albedo of a broken cloud field can be quite different from a similar, but homogeneous cloud layer (albedo bias; Barker 1992; Barker et al. 1996; Cahalan et al. 1994). This is a matter of concern since in all numerical climate studies the horizontal resolution is (and will be) much larger than the scale of the cloud inhomogeneity which, as a consequence, has to be parameterized.

What apparently is required is an insight in cloud-radiative properties, based on experimental evidence as a function of azimuthal and zenith angle (radiances) under conditions where simplifications such as the plane parallel approximation are likely to be invalid. Measurements of the angular distribution of scattered radiation (relative to the solar incidence) yield bidirectional reflectance distribution functions, which provide the required information on radiative scattering processes in clouds.

In this article we describe the design, development, calibration, validation, and airborne testing of a device that enables the measurement of scattered solar radiation in a number of directions relative to the solar incidence

Corresponding author address: Dr. Han van Dop, Institute for Marine and Atmospheric Sciences, Utrecht University, P.O. Box 80.005, TA Utrecht 3508, Netherlands.
E-mail: h.vandop@phys.uu.nl

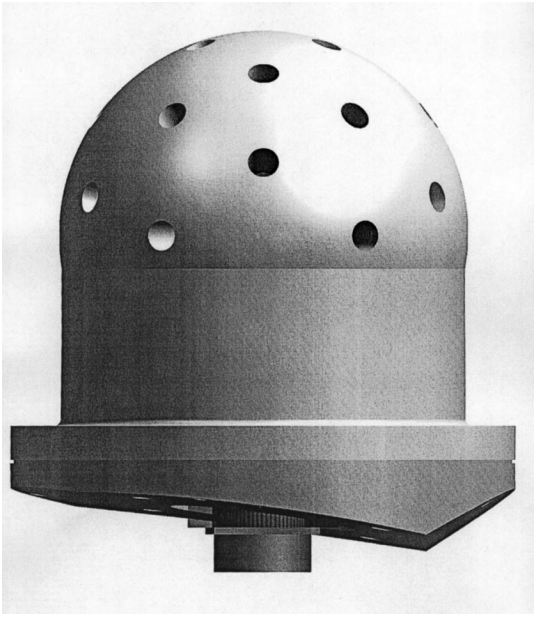

FIG. 1. The DIRAM sphere.

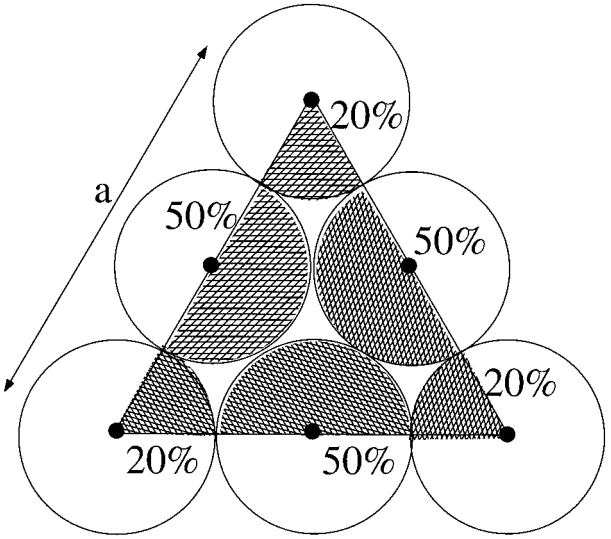

FIG. 2. One triangular face of the icosahedron. Each triangle contains six holes (three at the vertices and three at the middle of the sides). The circles are projections of the maximum (nonoverlapping) fields of view of each sensor. At each corner five icosahedron faces meet.

angle. The instrument is based on an original design by Davis et al. (1982), but equipped with sensors with a unique collimation system consisting of solid PERSPEX cylinders which combines simplicity with robustness and that yields both a strong light signal and a high discrimination with respect to the angle of incidence. The main difference with the earlier instrument is that Directional Radiance Distribution Measurement (DIRAM) device can operate with a small field of view, while maintaining a high signal-to-noise ratio (~1%), so that the angular distribution of the scattered radiation can be better resolved. The detecting photodiodes are sufficiently sensitive to measure radiance from cloudless regions of the sky.

b. Historical background

The design and scientific use of shortwave radiation measurements devices at the Institute for Marine and Atmospheric Research (IMAU) goes back to the 1980s. Instruments were designed to measure the radiation in vegetation (van der Hage 1984), the actinic flux above grassland (van der Hage 1992), and the horizontal component of radiation (van der Hage 1993). More recently, IMAU participated in a number of field experiments (Azores, Antarctic, and Netherlands) in order to study the interaction of clouds and radiation (Duynkerke and van Weele 1993; de Arellano et al. 1994; van der Hage and de Roode 1999). For this purpose a special sensor was designed and built to determine actinic fluxes as a function of height in cloudy and clear-sky conditions up to altitudes of 1.5 km under different surface albedos (van der Hage et al. 1994); van der Hage and de Roode 1999). The obtained results were used to validate radiative transfer models in clear-sky and overcast conditions. The combination of the current scientific interest in scattering of shortwave radiation by clouds and atmospheric (photo) chemistry, and our expertise with simple radiation instruments has initiated the development of the present DIRAM instrument.

2. The DIRAM instrument

a. Experimental design

The present concept (Fig. 1) consists of two hemispherical domes, one to be mounted on top of an aircraft and one under it. Each dome has 24 cylindrical holes (8-mm diameter); each hole contains a collimator and a detector.

To register the angular distribution of radiance in the atmosphere, a regularly distributed, spherical array of radiance sensors is required. To this end the holes were positioned in an icosahedral geometry of 20 equal triangles. Holes were drilled at each vertex and at the middle of each edge (see Fig. 2). In this way 42 sensors can be distributed over a full sphere in an approximately equidistant way. The distance between two adjacent sensors is $a/2$ when a is the length of an edge. When the fields of view of the six sensors on the triangular face are not allowed to overlap then the maximum aperture, ϕ (defined as the ratio of the radius of the circles in figure 2, $a/4$, and the radius of the enveloping sphere R) can then be found from

$$\sin\phi = \frac{a/4}{R} = \frac{a}{a\sqrt{2(5 + \sqrt{5})}} = 0.263. \qquad (1)$$

Thus, ϕ is just over 15°. With this aperture a coverage

TABLE 1. Nominal azimuthal (ψ^{up} and ψ^{down}) and zenith (θ) angles (°) for the sensors of the upward- and downward-oriented hemisphere, respectively. The values of the zenith angles are given relative to the axes of symmetry of both domes.

Position no.	ψ^{up}	ψ^{down}	θ
1	0	180	21
2	240	60	21
3	120	300	21
4	300	120	37.5
5	180	0	37.5
6	60	240	37.5
7	338	158	55
8	262	82	55
9	218	38	55
10	142	322	55
11	98	278	55
12	22	202	55
13	300	120	69
14	180	0	69
15	60	240	69
16	0	180	79
17	240	60	79
18	120	300	79
19	330	30	90
20	270	330	90
21	30	270	90

of 95% can be obtained. In Table 1 we have listed the azimuthal ψ and zenith angle θ of all holes.

b. Collimating system

The collimating system[1] consists of light-conducting PERSPEX (polymethyl-methacrylate) cylinders. This material has a very high transparency in the window 400–1200 nm. The aperture of the cylinders is determined by the length (l) of the tube and the diameter (d) of the collimating diaphragms (Fig. 3).

When both diaphragms have the same diameter d, we find: $\tan\varphi = 2d/l$, corresponding to an aperture of 10°. One extra diaphragm is required to screen reflections by the inside of the cylinder, since oblique reflection from the wall, even when the wall is treated with a low reflection coating, is a significant source of stray light. The extra diaphragm works two ways: it shields the view of the detector of the front part of the tube wall, and it prevents light with an angle of incidence $>\psi$ to enter the rear compartment of the tube (see Fig. 3a). Finally, light incident at angles between φ and ψ is reflected by the walls of the rear compartment but these reflections are screened from the detector by the detector diaphragm. The collimators were machined from a solid PERSPEX rod of 8-mm diameter, the sides covered with a black coating, attached to photodiodes and finally fitted in the holes in the DIRAM sphere.

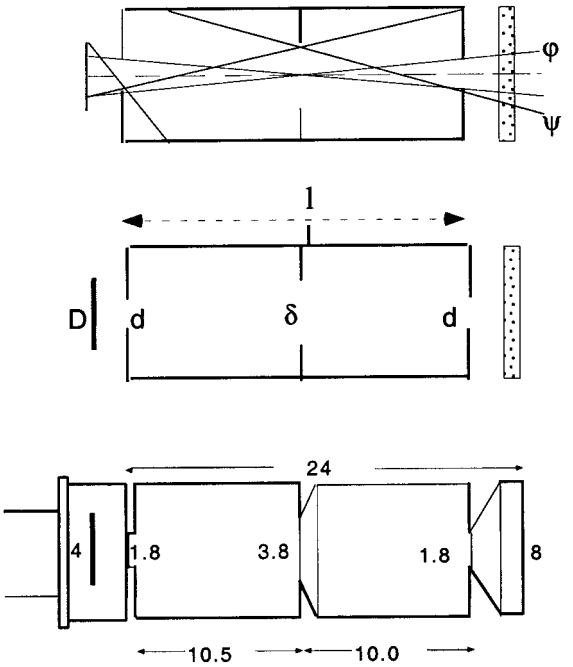

FIG. 3. A monolithic sensor. top: Optical geometry as prescribed by the diaphragms. middle: Conventional layout of the optical components. bottom: Actual construction, machined from a perspex rod with a photodiode attached (4). The dotted rectangle at the right symbolizes an emittor of radiation in all directions. The limiting angles φ and ψ are considered relative to the centerline. Here D, d, and δ denote the diameter of the detector, exit opening, and middle diaphragm, respectively. (Units: mm.)

3. Calibration

a. Viewing angles

A check of the azimuthal and zenith angles (see Table 1) of each of the 42 sensors after they were mounted in the holes in the aluminium spheres was made. This was done by mounting a laser in a spherical construction (~1-m radius) with the sphere positioned in the center. The laser could be moved in azimuthal and zenith directions. The direction of the laser beam was also adjustable. The position where the laser produced a maximum in the detector signal defined the viewing angle of the sensor. This could be done with an estimated accuracy of approximately 0.25° for ψ, while θ could be determined with an error of ~0.1°. In Fig. 4 we show (an average of) the measured deviations in azimuthal and zenith direction, respectively. Nearly all the sensors are placed into the holes in the spheres with an accuracy better than 1°. Only three sensors are misaligned just over 1° (no. 6 and no. 15 of the upper DIRAM sphere and no. 2 of the lower DIRAM sphere). The error in

[1] In the present monolithic version of DIRAM we have dropped an earlier idea of using optical fibers to collect the radiation and conduct it to the detector. Commercial fibers are designed to have large apertures and fibers must be quite thin (about 100 μm) to have an aperture smaller than the desired 15°. Unfortunately, the fibers collect only small amounts of light. We expected further problems with cloud droplets settling on the fiber entrance and disturbing the light path, which led us to abandon this approach.

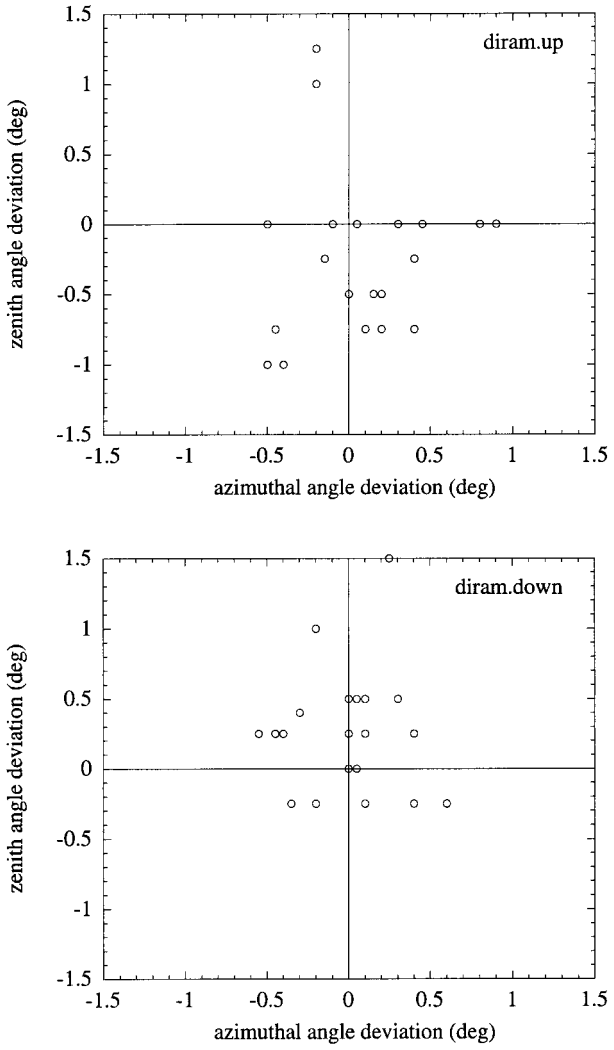

FIG. 4. Deviations (°) from azimuthal ψ and zenith θ direction for the (a) DIRAM-up sphere and the (b) DIRAM-down sphere.

the alignment is sufficiently small to enable the determination of angular radiation distributions.

b. Angular response and stray light

The angular response of each individual collimating system was determined by irradiating it with a laser beam as a function of incident angle α relative to the centerline of the sensor. A typical result of a collimator is given in Fig. 5. The full-width half-maximum is 7.14°, which is somewhat less than the geometrical aperture (10°) found in section 2b. There is a strong decrease in response toward large angles, up to 4–5 orders of magnitude for $\alpha > 35°$. In the absence of direct (solar) radiation, stray light[2] can be neglected. However, above

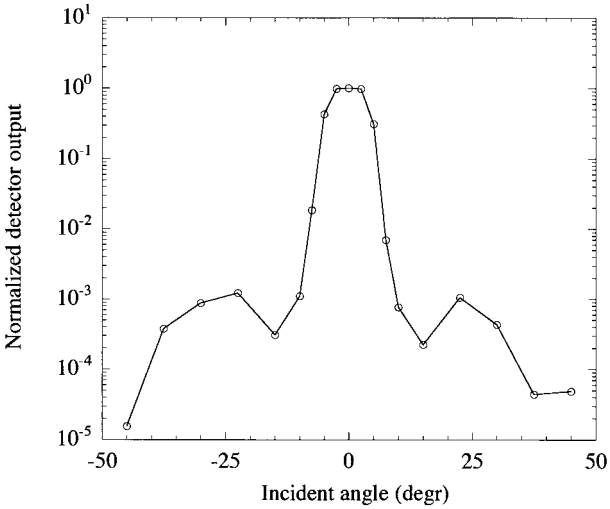

FIG. 5. The angular response of a collimator. The incident angle α is the direction of the laserbeam relative to the centerline of the sensor.

the clouds a correction to the signal may be necessary due to stray light from the sun. An estimate of this correction can be obtained as follows. Suppose that the direct solar radiation yields a signal in a sensor of $Sf_{\text{att}}(\alpha)$ (in V), where S is the signal when the sensor is pointed toward the sun[3] and $f_{\text{att}}(\alpha)$ is the attenuation factor depending on the solar incidence angle α on the sensor. The attenuation factor can be directly obtained from Fig. 5 and is defined as the ratio between the output at angle zero and α, respectively. Since S is of the order of 800 V, corrections up to 80 mV are required for angles larger than 10°. For smaller angles of incidence, that is, for sensors almost pointing toward the sun, larger corrections are required. For comparison we note that blue sky radiation yields a signal of ~25 mV in the detector. From clouds the signal is at least an order of magnitude larger. Correction for stray light must therefore be applied for sensors exposed to the sun.

It is clear that a sharply restricted field of view is required and we believe that the current construction is one of the few that yields narrow and restricted views. All collimators were tested and those with a significantly worse relative sensitivity or angular response than presented in Table 2 or Fig. 5 were rejected.

c. Sensitivity and dynamic range

On the surface of the DIRAM domes a circular groove is cut around each sensor. The function of these grooves is to enable the exact positioning of a reference light source on the optical axis of each sensor. A plain diffuse electric light source was applied to simultaneously illuminate both a ''reference sensor'' and any one sensor

[2] Stray light is defined as the contribution to the signal from light outside the field of view (7.14°) of the collimator.

[3] The size of the solar disk (in sr) is much smaller than the field of view.

TABLE 2. Relative sensitivity of a sample of 57 sensors. The ones marked with an asterisk were rejected if the deviation in sensitivity or in angular responses was much larger than average.

Sensor no. (i)	Position no.	Rel. sensitivity s_i	Sensor no. (i)	Position no.	Rel. sensitivity s_i
1	11u	0.95	31	1u	1.10
2	5d	1.09	32*	—	1.13
3	9u	1.10	33	12u	1.09
4	—	0.99	34	10d	0.96
5	2d	0.97	35	11d	1.14
6	4u	1.07	36	18d	1.04
7	2u	1.06	37	6u	1.12
8	16d	1.06	38	8d	1.07
9	15u	1.05	39	20u	1.04
10*	—	0.00	40*	—	1.06
11*	—	1.08	41	4d	1.05
12*	—	0.87	42	13d	0.98
13	20d	1.03	43	7u	0.97
14*	—	1.09	44	1d	1.03
15	—	1.08	45	17u	1.03
16	3u	1.04	46	21u	0.96
17	7d	1.01	47	18u	0.93
18*	—	1.09	48	5u	1.14
19	3d	1.04	49	14d	0.94
20	—	0.98	50	15d	1.08
21	19u	1.06	51*	—	0.95
22	21d	1.02	52	13u	1.04
23	9d	0.93	53	17d	1.00
24	10u	0.92	54	8u	1.09
25	—	1.10	55*	—	0.00
26	6d	0.97	56	16u	1.03
27	14u	1.06	57	12d	0.99
28	—	1.08			
29*	—	1.13			
30	19d	1.12			

in the DIRAM domes. For the reference sensor, an arbitrary sensor, similar to the ones in the dome was selected and kept in the laboratory. These measurements were repeated in reverse direction in order to remove possible linear trends in time of the light source, yielding a relative sensitivity factor s_i for each sensor i. The sensitivity factors are listed in Table 2. They may change in time due to aging of the diodes and the optics and therefore determination of sensitivity should be regularly repeated.

The absolute calibration was done by comparing the integrated DIRAM signal with the signal of a calibrated climatological global radiation meter (Kipp & Zonen CM5).[4] This was done in a campaign in France during the solar eclipse in August 1999. This occasion offered a large range of values of diffuse radiation, as we shall see shortly. Measurements were done in cloudy, almost overcast conditions. All observations where direct solar radiation was significant (i.e., when the solar disk was visible) were excluded from calibration. We denote the diffuse radiance by $R(\theta, \psi)$ (in W m^{-2} sr^{-1}). Then the global radiation G is by definition

[4] Kipp & Zonen B.V., P.O. Box 507, 2600 AM Delft, Netherlands; http:/www.kippzonen.com.

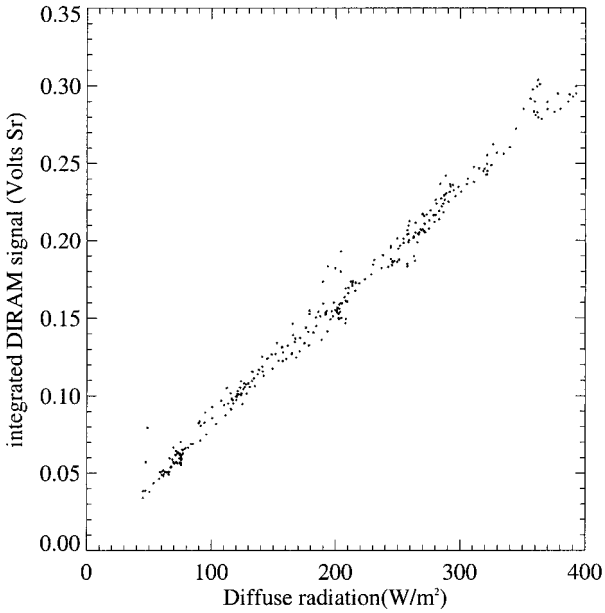

FIG. 6. The DIRAM integrated output (V_{tot}) against the signal of the Kipp & Zonen CM5 radiometer (G_D). Data were taken during the solar eclipse in France in Aug 1999.

$$G = \int_{\Omega} R(\theta, \psi) \cos\theta \, d\Omega, \tag{2}$$

where Ω denotes the solid angle ($=\sin\theta d\theta d\phi$). The integration extends to the upper hemisphere. The output V_i (in V) from a sensor i pointing in direction θ_i, ψ_i can be expressed as

$$V_i = s_i R(\theta_i, \psi_i) c \Delta\Omega, \tag{3}$$

where c is the conversion factor [V (W m^{-2})$^{-1}$], s_i's are the sensitivity factors (see Table 2) and $\Delta\Omega$ is the field of view of the sensor (sr). The latter was taken constant for each sensor and equal to 9.71×10^{-4} sr, corresponding with an aperture of 3.57° (the half-width half-maximum value from Fig. 5). The 21 values of the sensors of each dome, normalized with their relative sensitivity (V_i/s_i) were interpolated to a regular grid with N grid points, yielding $V_n (n = 1, N)$. After summation we obtain V_{tot} according to

$$V_{tot} = \sum_{n=1}^{N} V_n \cos\theta_n \sin\theta_n \Delta\theta\Delta\psi. \tag{4}$$

Note that the summation is over the N grid points of the interpolation grid and that $\Delta\theta$ and $\Delta\psi$ denote the grid size. The global radiation as measured by the DIRAM can now be expressed as

$$G_D = \frac{V_{tot}}{c\Delta\Omega}. \tag{5}$$

From the regression with the Kipp & Zonen global radiation radiometer the constant $c\Delta\Omega$ was determined (Fig. 6). The relationship is linear over a large range of

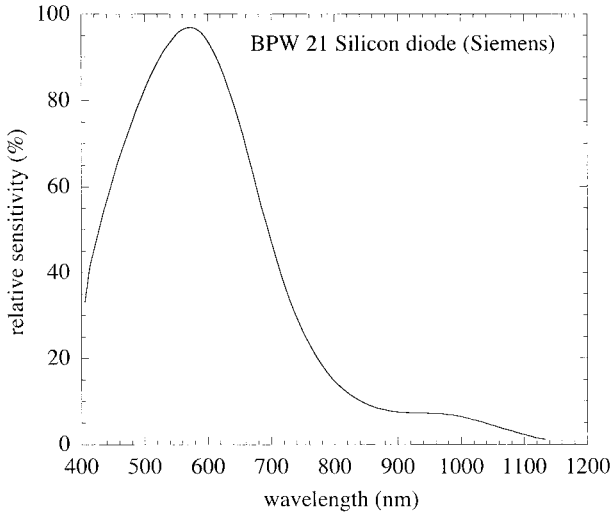

FIG. 7. The relative spectral response of a PERSPEX sensor with a BPW 21 photodiode.

values. The correlation coefficient is 0.994. From the regression a value for $c\Delta\Omega$ is obtained of 7.58×10^{-4} V sr $(\text{W m}^{-2})^{-1}$. Varying the number of grid points (N) or the interpolation method has little effect on the value of $c\Delta\Omega$. With the above value for the field of view, c equals 0.781 V $(\text{W m}^{-2})^{-1}$.

In the present DIRAM, BPW 21 diodes are used, which detect only a filtered fraction of the solar radiation. The spectral sensitivity of the DIRAM instrument has an optimum around 550 nm and a bandwidth of ~300 nm. The global radiation meter has a constant spectral sensitivity over the range from 400 to 1200 nm. Though the spectral response is different, we estimate that this does not affect the calibration significantly. (The spectral distribution of the solar radiation originating from areas close to the edge of the solar disk is considered to be not very different from that of the central part.)

d. Spectral response

The spectral sensitivity of the PERSPEX sensor is completely determined by the specifications of the BPW 21 (Siemens) silicon photodiode. This diode only responds to light in the range of 400–1200 nm, a range where PERSPEX is perfectly transparent (Touloukian et al. 1972). The spectral response is shown in Fig. 7. Weiss and Norman (1985) have shown that the relative spectral distribution in global radiation under a cloudy sky is practically identical to that under a clear sky, which justifies the assumption that the effects of different spectral responses of the Kipp & Zonen radiometer and the BPW 21 photodiode on the value of regression constant c are small in variable cloudiness. However, for blue sky conditions c may be somewhat different due to the deviating spectral response. This has to be looked into in further experiments.

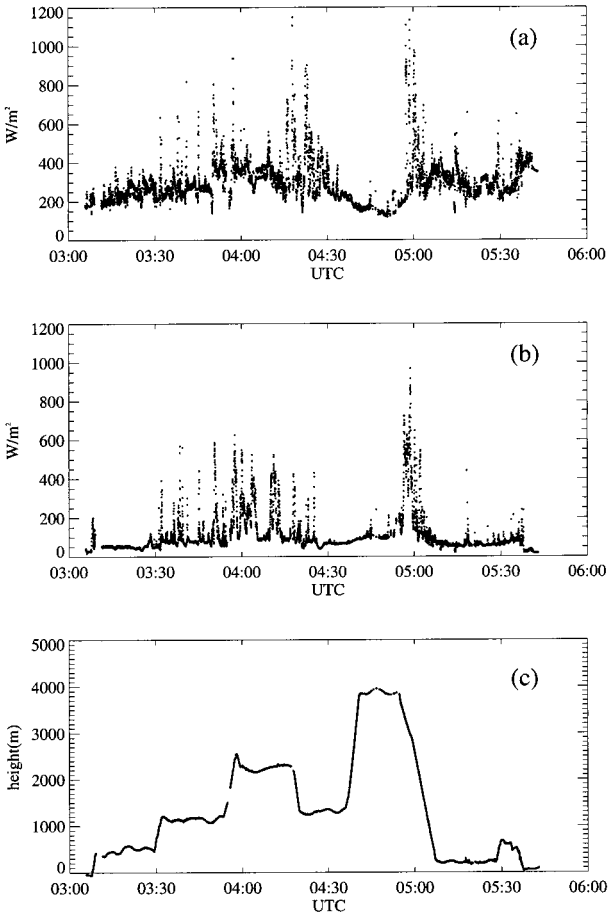

FIG. 8. Flight record of the integrated DIRAM signal (W m^{-2}): (a) top dome, (b) bottom dome, and (c) flight altitude (m).

4. Airborne test

For an initial field test the domes were mounted on board of a Dutch research aircraft (Cessna Citation). The system and datalogging were tested during a field campaign above the Indian Ocean (INDOEX). The 42 signals were simultaneously logged with a frequency of 1 Hz, which corresponds to a path length for a single detector of about 150 m (flying with a velocity of 150 m s^{-1}). As an example data from a flight over the Indian Ocean from Male (Maldives) to Colombo (Sri Lanka) are shown in Fig. 8. The signals of the sensors were integrated to obtain the total upward and downward radiative flux. The lower level of the signal corresponds to observations in a cloudless environments. We observe that in these conditions the diffuse radiation level recorded by the downward-looking dome (Fig. 8b) is significantly lower (50 W m^{-2}) than the radiation level of the upward-oriented dome (~200 W m^{-2}), consistent with the low albedo of the ocean surface. Peaks in the signal indicate that the aircraft is in a cloudy environment. For example, the cumulus fields during the descent around 0500 UTC are clearly visible.

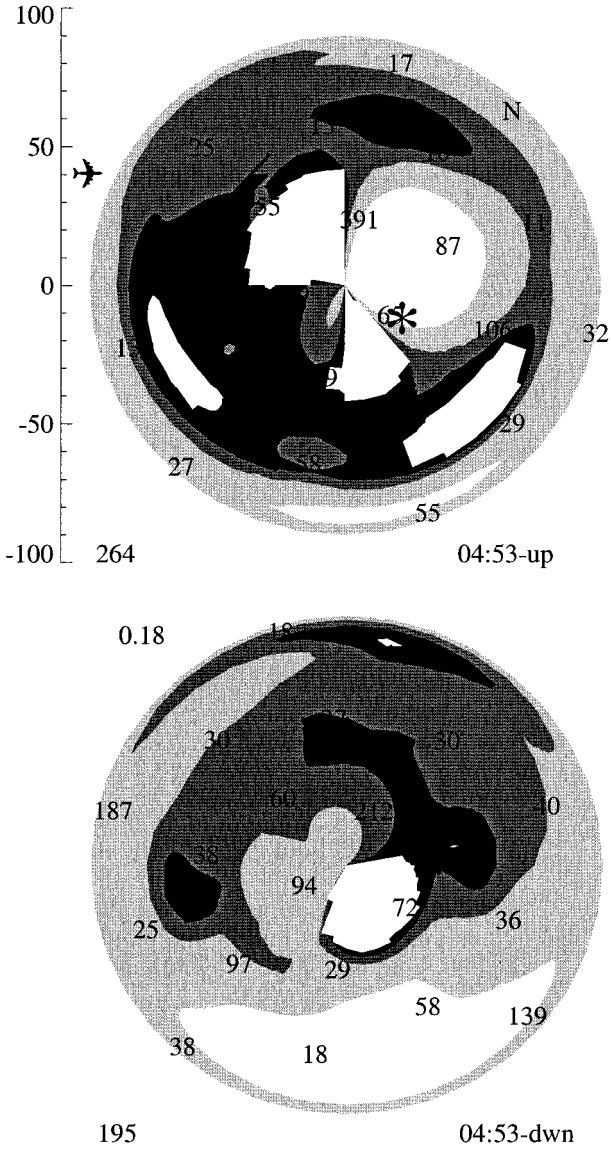

FIG. 9. Angular radiation distribution in geophysical polar coordinates, inferred from DIRAM (0453:00 UTC 21 Mar 1999) close to Colombo (Sri Lanka). The north is indicated with ''N,'' the position of the sun with a star. The center of the figures corresponds to the vertical upward and downward direction, respectively. Actual sensor values (W m^{-2}), on which the interpolation is based, are plotted at the proper locations. In the left-hand lower corners the integrated signal (W m^{-2}) is plotted. The lower graph (left, top) contains an estimate of the albedo (0.18), defined as the ratio of total upward and downward (including the direct solar) radiation. Along the vertical axis the flight altitude is indicated (in hundreds of meters). The shades indicate interpolated irradiance values (W m^{-2} sr^{-1}) white $>$ 150, light gray 50–150, dark gray 25–50, and black $<$25.

In Fig. 9 we have plotted an arbitrary interpolated radiation distribution observed at 0453:00 UTC. The figure shows the upper and lower hemisphere in a horizontal polar coordinate frame. The center points upward and downward, respectively, and the north is indicated by ''N.'' The position of the sun is indicated by a star and it is obvious that the sensors that are close to that direction receive the highest radiation. Levels are otherwise quite low, indicating a clear sky overhead. Only in southeastern direction at high zenith angles (close to the perimeter of the figure) radiation levels are enhanced, which indicate the presence of clouds. Note that the domes, which were placed at the bottom and top of the hull of the plane, respectively, follow the flight movements (heading, roll, pitch). These were continuously recorded and used to be able to present the observed data in the geophysical coordinates of Fig. 9.

We emphasize that these data are preliminary and collected without scientific purpose. They are presented only to show the technical features and operationality of the whole system. The instrument performed successfully during all six 2–3-h flights during this campaign.

5. Advantages and applications of DIRAM

The DIRAM instrument described in this paper combines robustness, simplicity, and versatility: it is a solid state instrument that does not contain moving parts. Moreover, it is insensitive to vibrations and to strongly changing temperatures. It contains only a small number of parts (the aluminium dome with 21 collimators and detectors). Versions with other spectral sensitivities can be easily fabricated by using different sensors or applying filters. Finally, the instrument is not expensive.

DIRAM can be operated in severe conditions mounted on an aircraft and at high altitudes. Other advantages are the high light yield (allowing for observations within clouds), and angular resolution which makes that it can operate also in sunny conditions. In that case, however, a correction for stray light should be applied.

The expectation is that the device is capable to measure bidirectional reflection functions, simultaneously from 42 directions and with a sampling frequency of up to 10 Hz.

The measurement of scattered radiation from clouds was the major objective in designing the instrument, but there are also other potentially interesting applications.

- The determination of the angular dependence of the albedo of the solid earth, including snow and ice surfaces (see, e.g., Reijmer et al. 1999).
- Providing ''ground truth'' for satellite radiometer measurements.
- By changing the detector (a relatively easy operation) scattering in other wavelength ranges or special narrow wavelength bands can be equally well investigated, since the light yield will remain sufficient. Only in the case of UV radiation should the PERSPEX collimators be replaced by quartz ones, which is perfectly viable but more expensive in production.
- The present angular resolution (field of view) is approximately 7°, which is considered sufficient for our purposes. By changing the geometry of the collimat-

ing system (applying longer tubes or making narrower diaphragms) the resolution can be improved if desired.
- In Gruffke et al. (1998, unpublished manuscript) a similar (ground based) device is described, which determines (among others) cloud speed (and height), which may also be a potential application of the DIR-AM device.

Currently further testing and calibration is carried out in the laboratory and at a nearby field (Cabauw) of the Dutch meteorological office (KNMI).

REFERENCES

Barker, H., 1992: Radiative transfer through clouds possessing isotropic variable extinction coefficient. *Quart. J. Roy. Meteor. Soc.,* **118,** 1145–1162.

——, B. Wielicki, and L. Parker, 1996: A parameterization for computing grid-averaged solar fluxes for inhomogeneous marine boundary layer clouds. Part II: Validation using satellite data. *J. Atmos. Sci.,* **53,** 2304–2316.

Cahalan, R., W. Ridgeway, W. Wiscombe, T. Belland, and J. Snider, 1994: The albedo of fractal stratocumulus clouds. *J. Atmos. Sci.,* **51,** 2434–2455.

Davis, J., C. Vogel, and S. Cox, 1982: Multidirectional photodiode array for the measurement of solar radiances. *Rev. Sci. Instrum.,* **53,** 667–673.

de Arellano, J. V.-G., P. Duynkerke, and M. van Weele, 1994: Tethered baloon measurements of actinic flux in a cloud-capped marine boundary layer. *J. Geophys. Res.,* **99,** 3699–3705.

Duynkerke, P. G., and M. van Weele, 1993: Actinic fluxes: The role of clouds in photodissociation. *Bound.-Layer Meteor.,* **62,** 417–432.

Los, A., and P. G. Duynkerke, 2001: Parametrization of solar radiation in inhomogeneous stratocumulus: Albedo bias. *Quart. J. Roy. Meteor. Soc.,* in press.

Reijmer, C., W. Knap, and J. Oerlemans, 1999: The surface albedo of the Vatnajökull ice cap, Iceland. A comparison between satellite-derived and ground-based measurements. *Bound.-Layer Meteor.,* **92,** 125–144.

Touloukian, Y., S. DeWitt, and X. Hernicz, 1972: *Thermophysical Properties of Matter.* Plenum, 1763 pp.

van der Hage, J., 1984: A small optical line sensor for radiation measurements in vegetation. *J. Exp. Botany,* **35,** 762–766.

——, 1992: A small optical line sensor for radiation measurements in vegetation. *Theor. Appl. Climatol.,* **46,** 173–177.

——, 1993: The horizontal component of solar radiation. *Agric. For. Meteor.,* **67,** 79–93.

——, and S. de Roode, 1999: An isotropic light sensor for measurements of visible actinic flux in clouds. *J. Atmos. Oceanic Technol.,* **16,** 1698–1701.

——, W. Boot, H. van Dop, P. Duynkerke, and J.V.-G. de Arellano, 1994: A photoelectric sensor suspended under a balloon for actinic flux measurements. *J. Atmos. Oceanic Technol.,* **11,** 674–679.

Weiss, A., and J. Norman, 1985: Partitioning solar radiation into direct and diffuse visible and near-infrared components. *Agric. For. Meteor.,* **34,** 205–213.